Hindawi Publishing Corporation
Research Letters in Materials Science
Volume 2007, Article ID 91796, 5 pages
doi:10.1155/2007/91796

Research Letter

Ferroelectric Properties of $Na_2Pb_2R_2W_2Ti_4V_4O_{30}$ (R = Dy, Pr) Ceramics

Piyush R. Das, Banarji Behera, R. N. P. Choudhary, and B. K. Samantray

Department of Physics and Meteorology, Indian Institute of Technology, Kharagpur 721302, India

Correspondence should be addressed to R. N. P. Choudhary, crnpfl@phy.iitkgp.ernet.in

Received 19 July 2007; Accepted 12 October 2007

Recommended by Chun-Hway Hsueh

The polycrystalline samples of $Na_2Pb_2R_2W_2Ti_4V_4O_{30}$ (R = Dy, Pr) were prepared by low-temperature, (i.e., at 650°C) solid-state reaction technique. The preparation conditions have been optimized using thermogravimetry analysis (TGA) technique. X-ray diffraction (XRD) studies of the compounds showed the formation of a single-phase orthorhombic crystal structure at room temperature. Studies of dielectric properties (ε_r and tan δ) of the compounds at frequencies 10, 100, and 1000 kHz in a wide temperature range (room temperature–500°C) exhibit ferroelectric phase transitions at 132°C for NPDWTV and at 122°C for NPPWTV of diffuse type. Ferroelectric properties of the materials are confirmed by polarization study.

1. INTRODUCTION

Ferroelectric oxides of tungsten bronze (TB) family are a class of important materials for applications in various electronic devices such as multilayer capacitors, transducers, actuators, ferroelectric random access memory and display, microwave dielectric resonators, pyroelectric detector, and so forth, owing to their unique electrooptic, nonlinear optic, photo refractive index, pyroelectric effect, and acoustic optic properties [1–7]. The TB structure consists of a skeleton framework of distorted BO_6 octahedra sharing corners in such a way that a variety of cations can be substituted at three different types of interstices (A, B, and C) of a general formula $(A_1)_2(A_2)_4(C_4)(B_1)_2(B_2)_8O_{30}$ where A-type (mono- or divalent) cations can be accommodated at different types of interstitial (A_1, A_2) sites. Tri- or pentavalent atoms are substituted at octahedral sites $B_1$and B_2 [8]. The C site (smallest interstice) is generally empty, and hence a general formula for filled tungsten bronze structure is $A_6B_{10}O_{30}$. Detailed literature survey reveals that a lot of work has been carried out on ferroelectric niobates and tantalates having TB structure [9–13]. Recently we have reported ferroelectricity in $Na_2Pb_2Sm_2W_2Ti_4Nb_4O_{30}$ [14], $Na_2Pb_2Nd_2W_2Ti_4Nb_4O_{30}$ [15], and $Na_2Pb_2R_2W_2Ti_4V_4O_{30}$ (R = Gd, Eu) [16]. To the best of our knowledge, no work on ferroelectric properties has been reported on the titled compounds. In view of this, we have synthesized new vanadates, $Na_2Pb_2R_2W_2Ti_4V_4O_{30}$ (R = Dy, Pr), and studied their structural, dielectric, and ferroelectric properties.

2. EXPERIMENTAL

The polycrystalline samples of $Na_2Pb_2R_2W_2Ti_4V_4O_{30}$ (R = Dy, Pr) (hereafter abbreviated as NPDWTV and NPPWTV) were prepared relatively at low temperature by a solid-state reaction technique.The high purity ingredients of Na_2CO_3, PbO, Dy_2O_3, Pr_2O_3, TiO_2, WO_3, and V_2O_5 were thoroughly mixed and ground. About 5 mg of the physical mixture of each compound were used for thermal analysis (PERKIN ELMER). The experiment was carried out in the temperature range of 50–850°C. Based on the thermal analysis, mixtures of the above were calcined at 650°C for 6 hours. X-ray powder diffraction data of calcined powder were collected using an X-ray powder diffractometer (Rigaku Miniflex) with CuK_α radiation ($\lambda = 1.5405$ Å) in a wide range of Bragg angles ($20^\circ \leq 2\theta \leq 80^\circ$) at a scanning rate of 3 deg./min. The fine powders of these compounds were palletized and sintered for 4 hours at 675°C in air. The pellets were electroded with high purity air-drying silver paste and dried at 150°C. The X-ray diffraction data were used to evaluate density (ρ) of the sample (loosely speaking theoretical density)

using the formula $\rho = (\sum A/N)/V$ (g/cm^3), $\sum A$ the sum of the atomic weights of all the atoms in the unit cell; N is the Avogadro's number and volume of the unit cell (cm^3). The evaluated density was compared with measured density ρ = (mass of the pellet sample/volume of the pellet sample) and percentage of porosity using the following relations:

$$\%\ \text{proposity} = \frac{\text{theoretical density} - \text{measured density}}{\text{theoretical density}} \times 100. \quad (1)$$

Microstructures of sintered pellets were recorded by JEOL JSM-5800 scanning electron microscope (SEM). The electrical properties of the sintered pellets were studied and the data were recorded using a computer-controlled Hioki 3532 LCR Hitester over a wide frequency range (10^2–10^6 Hz) at different temperatures (300–525°C). The piezoelectric coefficients (d_{33}) of the compounds were recorded on poled sample (4 kV/cm for 24 hours in the silicon oil) using piezometer (M/s. Piezo-test, Model: PM 200, London , UK). The hysteresis loops of the poled samples were obtained at room temperature using precision material analyzer (M/S. Radiant Technologies Inc., NM, USA) integrated with 4 kV voltage amplifiers.

3. RESULTS AND DISCUSSION

3.1. Thermal study

Figure 1 shows thermogravimetry analysis (TGA) and differential thermogravimetry (DTG) curves of physical mixtures of NPDWTV and NPPWTV. It is observed from TGA pattern that there is a mass loss of 1% from 50–200°C, followed by another mass loss of about 2% up to 450°C with a further small mass loss of about 0.5% up to 625°C in both the samples. The initial loss of mass up to 200°C may be due to the evaporation of surface absorbed moisture and relatively higher mass loss from 250–450°C may be due to the decomposition of carbonate with formation of intermediate reaction stage [17]. The final but very low loss of mass between 450–625°C may be due to the final thermal decomposition with formation of the desired compounds. Beyond that temperature, no appreciable mass loss in both the mixtures indicates the completion of reactions. These TGA observations are found to be in close agreement with the DTG patterns with appearance of peaks for every step of reaction as explained above [18].

3.2. Structural and microstructural studies

Figure 2(a) shows the XRD pattern of the compounds at room temperature. Both diffractograms are similar with small variations in the relative intensities and peak positions. The XRD peaks in both the samples, which are different from that of ingredients, suggest the formation of single-phase compounds. With the observed interplanar spacing (d_{obs}) of all the peaks of XRD patterns, unit cell parameters of the compounds were obtained in different crystal system, and unit cell configurations using a standard computer program package POWD [19]. An orthorhombic crystal system was selected for the compounds for which $\Sigma\Delta d = \Sigma(d_{obs} - d_{cal})$ was found to be the minimum. The least-squares refined unit cell parameters are a = 18.8696(12) Å, b = 19.8915(12) Å, c = 3.8018(12) Å, and volume V = 1470.70 Å^3 for NPDWTV; and a = 19.7863(7) Å, b = 19.9355(7) Å, c = 3.7269(7) Å, and V = 1402.25 Å^3 for NPPWTV (estimated error in parenthesis). The crystallite size (P) of the compound was calculated from a few reflection peaks widely spread in 2θ (Bragg angles) range using Scherrer's equation $P_{hkl} = k\lambda/\beta_{1/2}\cos\theta$ [20], where k = 0.89, λ = 1.5405 Å, $\beta_{1/2}$= half peak-width. The broadening of reflections due to mechanical strain and other effects has been ignored. The average crystallite size of the NPDWTV and NPPWTV are found to be 26 nm and 25 nm, respectively. The values of theoretical density of the compounds were estimated to be ~4.72 and 4.48 g/cc, and the corresponding (bulk) densities of the pressed pellets were ~4.4 and 4.2 g/cc. The experimental densities were 93 and 94% of theoretical densities for NPDWTV and NPPWTV, respectively.

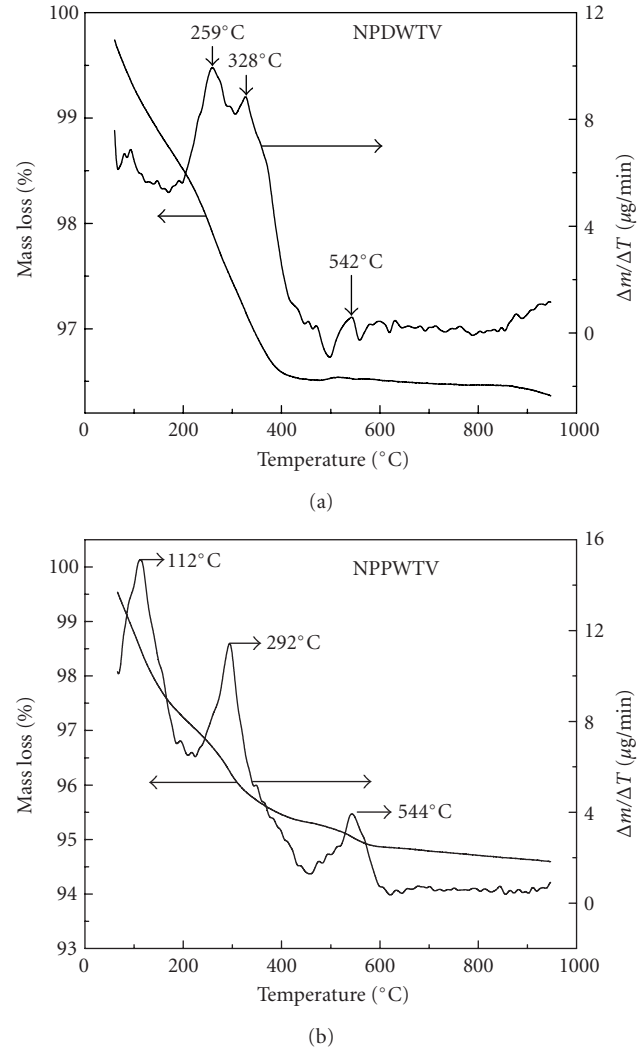

Figure 1: TG/DTG curves of NPDWTV and NPPWTV.

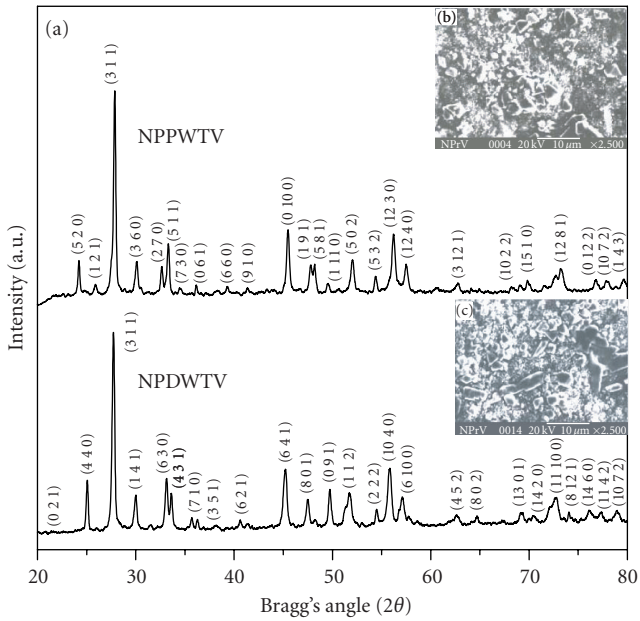

FIGURE 2: (a) X-ray diffraction patterns of NPDWTV and NPPWTV at room temperature and SEM micrographs of (b) NPDWTV and (c) NPPWTV.

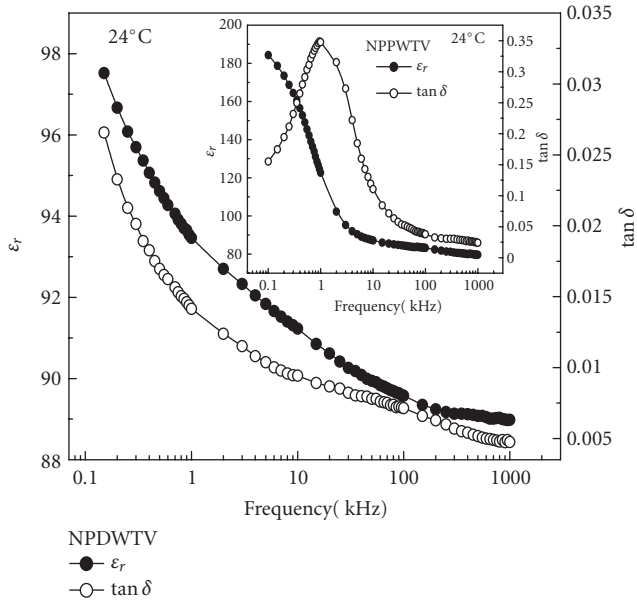

FIGURE 3: Variation of relative dielectric constant (ε_r) and loss tangent (tan δ) of NPDWTV and NPPWTV as a function of frequency at room temperature.

Figures 2(b) and 2(c) show the SEM micrographs of the sintered pellets of NPDWTV and NPPWTV. The nature and shape of grains show polycrystalline characteristic of the samples with less porosity. The grains are elongated and uniformly distributed over the entire surface of the samples. The grain sizes of NPDWTV are in the range of 2–10 μm and of NPPWTV in the range of 1–5 μm.

3.3. *Dielectric study*

The variation of relative dielectric constants (ε_r) and loss tangent (tan δ) at room temperature of both the compounds with frequency (10^2–10^6 Hz) is shown in Figure 3. It is observed that both the parameters decrease with increase in frequency, which is a normal behavior of dielectric/ferroelectric materials. But in the case of NPPWTV, the tanδ increases up to 1 kHz and thereafter decreases. This suggests that the material shows relaxation behavior at room temperature. Both the compounds have low dielectric constant (i.e., 81 and 80 at 10 kHz for NPDWTV and NPPWTV, resp.) at 24°C. This low value of dielectric constant of ferroelectrics may be due to the highly chemical covalent bonds with complex structure and no local electrical conduction [21], where ionic, dipolar, and interfacial polarization is insignificant. The electronic polarization is always present in these materials. Another effect for low dielectric constant may be due to the presence of porosity in the materials, since air has the lowest dielectric constant.

Figure 4 shows the temperature dependence of ε_r and tanδ at 10, 100, 1000 kHz for NPDWTV and NPPWTV, respectively. It is observed that ε_r increases gradually with rise in temperature to its maximum value (ε_{max}), and then decreases for both the compounds. The dielectric anomalies are obtained at 132 and 122°C for NPDWTV and

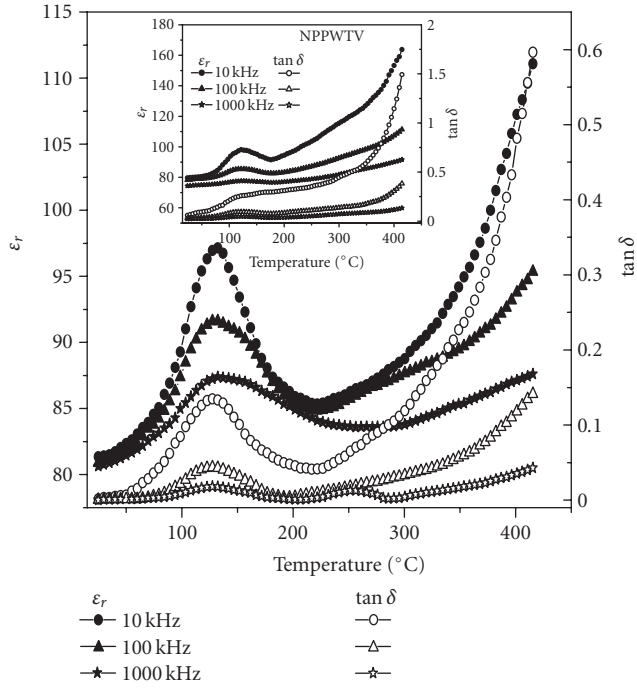

FIGURE 4: Variation of relative dielectric constant (ε_r) and loss tangent (tanδ) of NPDWTV and NPPWTV (inset) as a function of temperature.

NPPWTV, respectively. These anomalies may be associated with ferroelectric-paraelectric phase transition, which will be confirmed by appearance of hysteresis loops (as shown in the later section). On further increasing in temperature,

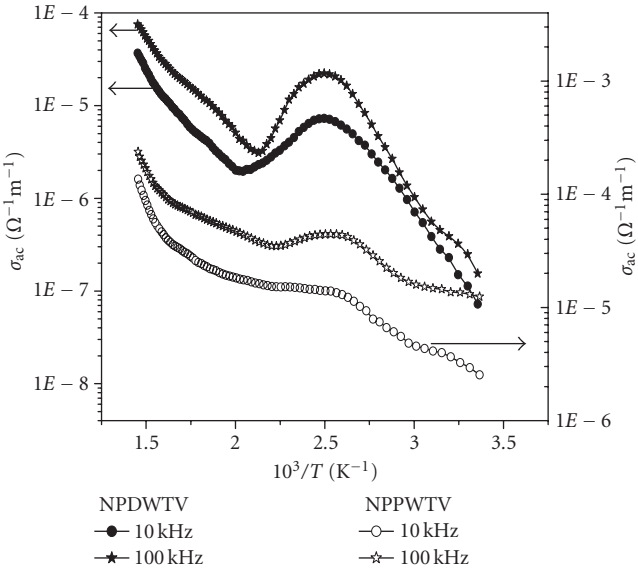

Figure 5: Variation of σ_{ac} with inverse of absolute temperature of NPDWTV and NPPWTV at 10 and 100 kHz.

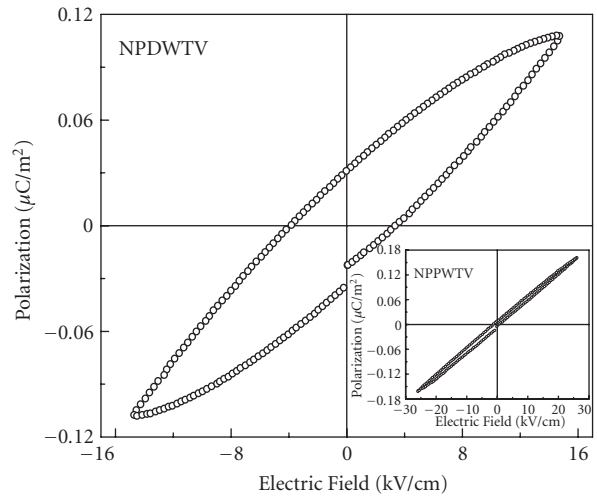

Figure 6: Ferroelectric hysteresis loops of NPDWTV and NPPWTV at room temperature.

ε_r increases faster. In high temperature region, higher value of ε_r may be due to space charge polarization, which comes from mobility of ions and imperfection in the materials. It has also been observed that ε_{max} is independent of frequency, which suggests that these compounds have no relaxor behavior. The maximum values of dielectric constant at $T_c(\varepsilon_{max})$ for 10, 100, and 1000 kHz are 97, 92, and 87 for NPDWTV and the corresponding values for NPPWTV are 98, 85, and 78, respectively. It is observed that there are anomalies in $\tan\delta$ also (near T_c) in both the compounds. The corresponding maximum values of $\tan\delta$ at 10, 100, 1000 kHz are 0.13, 0.43, and 0.02 for NPDWTV and 0.25, 0.09, and 0.04 for NPPWTV. The higher value of $\tan\delta$ at high temperature may be due to the (i) enhancement of conductivity and (ii) reduction in the ferroelectric domain wall contribution. The dielectric peak was found to be broadened indicating the existence of diffuse phase transition. The diffusivity (γ) in the compounds was calculated using an expression $\ln(1/\varepsilon_r - 1/\varepsilon_{max}) = \ln K + \gamma\ln(T - T_c)$ [22], where ε_{max} is the value of ε_r at T_c and K is an arbitrary constant. For NPDWTV and NPPWTV, value of γ was found to be 1.37 and 1.50, respectively, at 10 kHz.

3.4. AC conductivity

The AC conductivity (σ_{ac}) of the samples was evaluated from the dielectric data using the empirical relation: $\sigma_{ac} = \varepsilon_r\varepsilon_o\omega\tan\delta$, where ε_o is the vacuum dielectric constant and ω is the angular frequency. Figure 5 shows the temperature dependence of AC conductivity of the samples at 10 kHz. A linear variation of σ_{ac} over a wide temperature range supports the existence of thermally activated transport properties of materials, which obeys the Arrhenius equation $\sigma_{ac} = \sigma_0\exp(-E_a/kT)$, where the symbols have their usual meanings. The anomalies in σ_{ac} at 132 and 122°C for NPDWTV and NPPWTV, respectively, correspond to the anomalies observed in our dielectric study. The activation energy (E_a) of the samples (calculated using Arrhenius equation) is found to be 0.40 eV in the ferroelectric phase ($<T_c$) and 0.53 eV in the paraelectric phase ($>T_c$) for NPDWTV, and 0.23 eV in the ferroelectric phase, and 0.44 eV in the paraelectric phase for NPPWTV. The activation energy varies from 0.23–0.40 eV in the low frequency limit. This is ascribed to the creation of electrons arising from the transition of valence state of vanadium. The conductivity became almost independent of temperature in the intermediate range, and hence this region may correspond to the saturation of liberation of electrons. At higher frequencies the activation energy is larger than that of low frequencies. Above T_c, there is an abrupt change in the slope of Arrhenius plot. The shape of the curve is steep and the activation energy was found varying from 0.44–0.53 eV. This is associated with the oxygen ion vacancies that are created due to the variable valence state of vanadium (i.e., V^{4+}-V^{5+}) at higher temperatures, which contributes to the conduction process. The hopping conduction and dielectric properties may be responsible for the low value of activation energy at low temperature (in ferroelectric phase). The valence state is likely to change not more than one unit, and will be a result of the formation of oxygen ion vacancies. Therefore, the conductivity may be of mixed type (i.e., ionic-polaronic and space charge) [23–25]. This study clearly demonstrates that the conductivity mechanism is due to the oxygen ion vacancies at higher temperatures.

3.5. Hysteresis study

The ferroelectric hysteresis loops of poled samples of NPDWTV and NPPWTV were recorded at room temperature with the application of electric fields of 15 and 26 kV/cm, respectively (Figure 6). The nature of hysteresis loops indicates that the samples are lossy. The maximum polarizations P_{max} are found to be 0.108 and 0.162 μC/m^2 and

remanent polarization ($2P_r$) to be 0.066 and 0.022 μC/cm^2 (at an applied electric field of 15 and 26 kV/cm) for NPDWTV and NPPWTV, respectively. The piezo-coefficient (d_{33}) of both the compounds is found to be 4. The existence of hysteresis loops and piezo-coefficient confirm that the investigated samples are ferroelectric in nature.

4. CONCLUSION

The polycrystalline samples of NPDWTV and NPPWTV were synthesized relatively at low temperature by a solid-state reaction technique. The preparation conditions of sample were optimized by thermogravimetry analysis. X-ray analysis exhibits the formation of single-phase orthorhombic crystal structure of the compounds at room temperature. Both the compounds have a dielectric anomaly at 132 and 122°C for NPDWTV and NPPWTV, respectively, suggesting possible ferroelectric-paraelectric phase transition of diffuse type. The appearance of hysteresis loop at room temperature confirmed ferroelectric properties of the materials at room temperature. The conductivity study shows that the conduction process in the materials is due to the oxygen ion vacancies at higher temperatures, and the conductivity may be of mixed type (i.e., ionic-polaronic and space charge).

REFERENCES

[1] R.-J. Xie, Y. Akimune, R.-P. Wang, K. Matsuo, T. Sugiyama, and N. Hirosaki, "Spark plasma sintering of tungsten bronze $Sr_{2-x}Ca_xNaNb_5O_{15}$ (x = 0.1) piezoelectric ceramics: I, processing and microstructure," *Journal of the American Ceramic Society*, vol. 85, no. 11, pp. 2725–2730, 2002.

[2] C. Huang, A. S. Bhalla, and R. Guo, "Measurement of microwave electro-optic coefficient in $Sr_{0.61}Ba_{0.39}Nb_2O_6$ crystal fiber," *Applied Physics Letters*, vol. 86, no. 21, Article ID 211907, 3 pages, 2005.

[3] Y. Yuan, X. M. Chen, and Y. J. Wu, "Diffused ferroelectrics of $Ba_6Ti_2Nb_8O_{30}$ and $Sr_6Ti_2Nb_8O_{30}$ with filled tungsten-bronze structure," *Journal of Applied Physics*, vol. 98, no. 8, Article ID 084110, 5 pages, 2005.

[4] M. R. Ranga Raju, R. N. P. Choudhary, and H. R. Rukmini, "Diffuse phase transition in $Sr_5RTi_3Nb_7O_{30}$ (R = La, Nd, Sm, Gd and Dy) ferroelectric ceramics," *Ferroelectrics*, vol. 325, pp. 25–32, 2005.

[5] J.-H. Ko, S. Kojima, S. G. Lushnikov, R. S. Katiyar, T.-H. Kim, and J.-H. Ro, "Low-temperature transverse dielectric and pyroelectric anomalies of uniaxial tungsten bronze crystals," *Journal of Applied Physics*, vol. 92, no. 3, pp. 1536–1543, 2002.

[6] M. Lee, R. S. Feigelson, A. Liu, and L. Hesselink, "Photorefractive properties of tungsten bronze ferroelectric lead barium niobate ($Pb_{1-x}Ba_xNb_2O_6$) crystals," *Journal of Applied Physics*, vol. 83, no. 11, pp. 5967–5972, 1998.

[7] K. S. Rao, T. N. V. K. V. Prasad, N. Vallisnath, and V. R. K. Murthy, "Pyroelectric ferroelectric and resistivity studies on samarium modified barium strontium sodium niobate ceramics," *Botswana Journal of Technology*, vol. 12, no. 2, pp. 1–7, 2003.

[8] P. B. Jamieson, S. C. Abrahams, and J. L. Bernstein, "Ferroelectric tungsten bronze-type crystal structures. I. Barium strontium niobate $Ba_{0.27}Sr_{0.75}Nb_2O_{5.78}$," *Journal of Chemical Physics*, vol. 48, no. 11, pp. 5048–5057, 1968.

[9] A. K. Singh and R. N. P. Choudhary, "Study of ferroelectric phase transition in $Pb_3R_3Ti_5Nb_5O_{30}$ (R = rare earth ion) ceramics," *Ferroelectrics*, vol. 325, pp. 7–14, 2005.

[10] M.-S. Kim, J.-H. Lee, J.-J. Kim, H. Y. Lee, and S.-H. Cho, "Microstructure evolution and dielectric properties of $Ba_{5-x}Na_{2x}Nb_{10}O_{30}$ ceramics with different Ba-Na Ratios," *Journal of Solid State Electrochemistry*, vol. 10, no. 1, pp. 18–23, 2006.

[11] L. Fang, H. Zhang, T. H. Huang, R. Z. Yuan, and H. X. Liu, "Preparation, structural, and dielectric properties of $Ba_5YZnM_9O_{30}$(M = Nb, Ta) ceramics," *Journal of Materials Science*, vol. 40, no. 2, pp. 533–535, 2005.

[12] B. Behera, P. Nayak, and R. N. P. Choudhary, "Structural, dielectric and electrical properties of $NaBa_2X_5O_{15}$ (X = Nb and Ta) ceramics," *Materials Letters*, vol. 59, no. 27, pp. 3489–3493, 2005.

[13] V. Hornebecq, C. Elissalde, J.-M. Reau, and J. Ravez, "Relaxations in new ferroelectric tantalates with tetragonal tungsten bronze structure," *Ferroelectrics*, vol. 238, no. 1, pp. 57–63, 2000.

[14] P. R. Das, R. N. P. Choudhary, and B. K. Samantray, "Diffuse ferroelectric phase transition in $Na_2Pb_2Sm_2W_2Ti_4Nb_4O_{30}$ ceramics," *Materials Chemistry and Physics*, vol. 101, no. 1, pp. 228–233, 2007.

[15] P. R. Das, R. N. P. Choudhary, and B. K. Samantray, "Diffuse ferroelectric phase transition in $Na_2Pb_2Nd_2W_2Ti_4Nb_4O_{30}$ ceramic," to appear in *Journal of Alloys and Compounds*.

[16] P. R. Das, R. N. P. Choudhary, and B. K. Samantray, "Diffuse phase transition in $Na_2Pb_2R_2W_2Ti_4V_4O_{30}$ (R= Gd, Eu) ferroelectric ceramics," *Journal of Physics and Chemistry of Solids*, vol. 68, no. 4, pp. 516–522, 2007.

[17] G. A. Kolta, I. F. Hewaidy, N. S. Felix, and N. N. Girgis, "Reactions between sodium carbonate and vanadium pentoxide," *Thermochimica Acta*, vol. 6, no. 2, pp. 165–177, 1973.

[18] J. M. Luiz, J. R. Matos, I. Giolito, and M. Ionashiro, "Thermal behaviour of the basic carbonates of lanthanum-europium," *Thermochimica Acta*, vol. 254, pp. 209–218, 1995.

[19] E. Wu, "POWD, an interactive powder diffraction data interpretation and indexing program ,version 2.5," School of Physical Sciences, Finders University of South Australia, Bedford Park, Australia.

[20] H. P. Klug and L. E. Alexander, *X-Ray Diffraction Procedures: For Polycrystalline and Amorphous Materials*, John Wiley & Sons, Chichester, UK, 1974.

[21] S. Seraji, Y. Wu, M. Forbess, S. J. Limmer, T. Chou, and G. Cao, "Sol-gel-derived mesoporous silica films with low dielectric constants," *Advanced Materials*, vol. 12, no. 22, pp. 1695–1698, 2000.

[22] S. M. Pilgrim, A. E. Sutherland, and S. R. Winzer, "Diffuseness as a useful parameter for relaxor ceramics," *Journal of the American Ceramic Society*, vol. 73, no. 10, pp. 3122–3135, 1990.

[23] G. Deng, G. Li, A. Ding, and Q. Yin, "Evidence for oxygen vacancy inducing spontaneous normal-relaxor transition in complex perovskite ferroelectrics," *Applied Physics Letters*, vol. 87, no. 19, Article ID 192905, 3 pages, 2005.

[24] B. Behera, P. Nayak, and R. N. P. Choudhary, "Dielectric anomaly in $LiCa_2V_5O_{15}$ ceramics," *Materials Letters*, vol. 61, no. 18, pp. 3859–3862, 2007.

[25] A. Molak, E. Talik, M. Kruczek, M. Paluch, A. Ratuszna, and Z. Ujma, "Characterisation of $Pb(Mn_{1/3}Nb_{2/3})O_3$ ceramics by SEM, XRD, XPS and dielectric permittivity tests," *Materials Science and Engineering B*, vol. 128, no. 1–3, pp. 16–24, 2006.